

Keywords: civil engineering and transport; AHSS steel welding; bending test; metallographic structure; mechanical resistance; Method of Fundamental Solutions

**Bożena SZCZUCKA-LASOTA¹, Anita UŚCIŁOWSKA², Tomasz WĘGRZYN^{3*},
Bogusław ŁAZARZ⁴, Jan PIWNIK⁵**

PLASTICITY PROPERTIES OF ADVANCED HIGH-STRENGTH STEEL WELD CONSTRUCTION OF TRANSPORT MEANS – SIMULATION BY THE MESH-FREE METHOD

Summary. Advanced high-strength steel (AHSS) is being used increasingly often in the structure of means of transport. Welds made of these steels can crack in the heat-affected zone (HAZ) and have inferior mechanical properties compared to the base material. The goal of this paper was to solve the technological and material problem of obtaining high-strength thin-walled welded structures of AHSS steel designed for heavily loaded elements of transport means. The novelty of the article is its presentation of a modified welding process which enables a high-strength structure of the obtained joint to be obtained without welding defects and incompatibilities. Copper backing was selected as an effective method of heat dissipation in the process, and, using the basic solutions method, the leverage of a heat flow process in the weld method deposit (WMD) was checked after cooling down the substrate. The fundamental solutions method was used to determine the optimal shape of the backing. It has been shown that the new backing affects the structure and mechanical properties of welds. In order to verify the newly developed method, tensile tests of the obtained joint were carried out, the hardness was assessed, the metallographic structure was analyzed, and non-destructive tests were performed. The developed material and technological solution were used, for example, for the construction of the arm element of the mobile platform.

1. INTRODUCTION

Because of the update to the regulations on exhaust emissions in motor vehicles, manufacturers are obliged to introduce additional components to motor vehicles, such as particulate filters, catalytic converters, exhaust system components (e.g. nozzles) and or auxiliary silencers, which significantly increase their weight. In trucks, the difference can be as much as 250 kg.

Due to new trends, steel producers are producing new materials with improved mechanical properties in response to the needs of, inter alia, the automotive industry. The use of a new generation of high-strength steels for transport would allow for significant reductions in vehicle weight, fuel consumption and harmful gas emissions to the environment. The welding of these steels is not well understood yet.

¹ Silesian University of Technology; 8 Krasińskiego, 40-019 Katowice, Poland; e-mail: bozena.szczucka-lasota@polsl.pl; orcid.org/0000-0003-3312-1864

² Poznan University of Technology; 3 Piotrowo, 60-965 Poznan, Poland; e-mail: anita.uscilowska@put.poznan.pl; orcid.org/0000-0002-0805-8210

³ Silesian University of Technology; 8 Krasińskiego, 40-019 Katowice, Poland; e-mail: tomasz.wegrzyn@polsl.pl; orcid.org/0000-0003-2296-1032

⁴ Silesian University of Technology; 8 Krasińskiego, 40-019 Katowice, Poland; e-mail: boguslaw.lazarz@polsl.pl; orcid.org/0000-0003-3513-8117

⁵ Wyższa Szkoła Bankowa w Gdańsku; aleja Grunwaldzka 238A, 80-266 Gdańsk, Poland; e-mail: j.piwnik@pb.edu.pl; orcid.org/0000-0001-9436-7142

* Corresponding author. E-mail: tomasz.wegrzyn@polsl.pl

Welded joints of these steels are mainly characterized by weaker strength than the base material. Continuous efforts to reduce the weight of manufactured structures should be related to the passive safety of vehicles [1]. In the automotive industry, advanced high-strength steel (AHSS) is becoming more and more useful. AHSS could be used in the structure of various vehicle elements due to its high tensile strength, high yield strength, high ductility, high good formability, and weldability.

Another significant advantage of AHSS is its relatively easy formation and machining. AHSSs are suitable for use in the automotive sector because they offer the possibility of reducing the mass of car body and load-bearing elements with a contemporary increase of mechanical properties in comparison with low-alloy steels and welds [5-6]. The main advantage of AHSS is its relatively low price due to the small number of alloying elements. AHSS is still considered difficult to weld because of the martensite structure [7].

There is a growing demand for the creation of new materials and welding technologies in structures for the needs of the new scientific discipline of transport and civil engineering. A good example of this application may be observed on the mobile platform (which is an important means of transport used in civil engineering). Materials intended for mobile platforms should have high strength (over 1050 MPa) [6]. However, AHSS welds are characterized by half the strength of the base material [7-9]. In order to slim down the structure of vehicles and other means of transport, materials of very high strength with thin sheet thicknesses are now being used for the elements of various vehicle structures (Fig. 1).

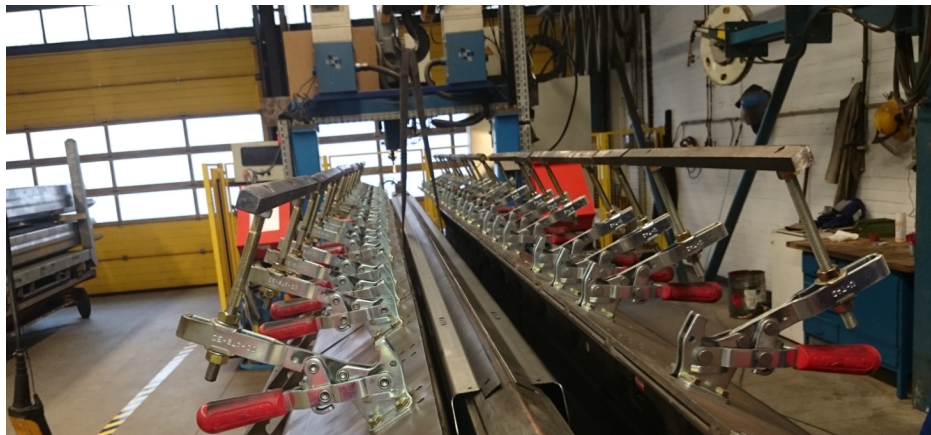


Fig. 1. Positioning of the elements of mobile platforms on a forming copper backing before welding

All welding parameters, including those related to heat supply and dissipation, must be controlled to obtain the most favourable joint. This matter is related to obtaining good properties of the weld (e.g. good relative elongation and good impact toughness) [11-13]. During the welding process, it is important that heat is dissipated quickly, which can be achieved by using copper backings (Fig. 1). There is an increasing interest in the use of welding backings (washers) in various means of transport. A serious difficulty of AHSS welding is related to their cracking, both at the fusion zone and the heat-affected zone (HAZ). Another disadvantage of AHSS is that the strength of the weld is lower than the strength of the base material. For instance, the tensile of Docol 1200M steel is 1230 MPa, whereas the joint strength is nearly half that (710 MPa). The main differences in these properties are the consequence of the chemical composition of the base material and weld [14-17]. The weld metal deposit mainly contains martensite, bainite and coarse ferrite, while the base material contains mainly martensite and more fragmented ferrite [7]. It was decided to use copper welding washers with a high heat transfer coefficient of 400 W/(mK) in order to change the structure of the joint. Ceramic washers may not be used to cool welds for AHSSs due to their very low heat transfer coefficient of 2 W/mK. This article aims to verify and validate the influence of cooling backings (washers) on the structure and properties of welds because their use might affect the alteration of austenite in AHSSs. The novelty of this article is its computer simulations, which can be used to predict the welding parameters to obtain joints with the desired properties. The proposed numerical method based on meshless methods was found to be an appropriate tool.

2. MATERIALS AND METHODS

2.1. Materials

Docol 1200M steel samples with dimensions of 800 mm × 160 mm × 1.8 mm were made with or without forming copper backings (washers):

- Sample S1, face connector, Docol 1200M steel, material thickness of 1.8 mm, MAG (Metal Active Gas) welding process in the low welding position (PA), without a backing
- Sample S2, face connector, Docol 1200M steel, material thickness of 1.8 mm, the same welding process but using a forming copper backing.

Welding was performed using a gas shield mixture (82% Ar + 18% CO₂) with a gas flow of 13.5 l/min. The unit energy of the process was at the level of 33 kJ/mm. The chemical composition of the tested Docol 1200M steel is provided in Table 1.

Table 1

Composition of Docol 1200M steel [13]

C%	Si%	Mn%	P%	S%	Al%	Nb%	V%	Ti%
0.11	0.2	1.7	0.010	0.002	0.40	0.15	0.05	0.025

When analyzing the chemical composition of a material, a 10-fold increase can be noticed in the aluminum and titanium content in relation to C-Mn steel, which is commonly used in the construction of the load-bearing components of vehicles. This has an impact on the steel's strength increase. Table 2 presents the main properties of Docol 1200M steel used in the tests.

Table 2

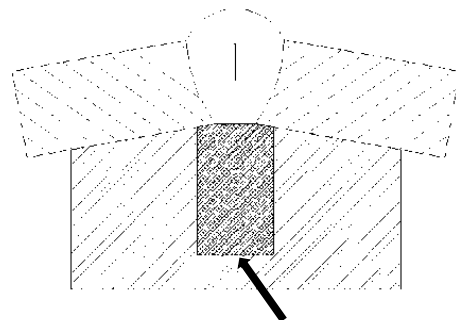
Mechanical properties of Docol 1200M steel [13]

Yield strength, F _y , MPa	Tensile strength, F _u , MPa	Elongation at the break of the sample with thickness	
		<3 mm, A ₈₀ %	≥3 mm, A ₅ %
930	1220	11	13

Butt joints of Docol 1200 M were made according to the requirements of EN 15614-1 standards. The preparation of the samples is shown in Fig. 2. The welding of samples S1 and S2 was very similar. S2 was formed using copper backings. The copper washer is part of a larger assembly, which is clearly shown in Fig. 2.



S2 - welding without copper backings



S2 - welding with copper backings

Fig. 2. Groove shape of S1 and S2 [16]

The groove shape clearance was the same in both cases (0.8 mm). The joint was made at an angle of 135°. The cross-section of the copper insert throughout the backing (washer) can be approximated by the dimensions of a 5 × 10 mm rectangle. These wires containing Ni and Mo had a positive influence on the plastic properties (especially impact toughness) of the weld [8]. The main welding process parameters are provided in Table 4.

The washer used in the tests had the same length as the samples (1 m), and its cross-section was similar to a rectangle measuring 30 mm × 20 mm. The dimensions of the copper backing were selected

using the method of fundamental solutions. All samples were welded with wire UNION X96 (i.e. EN ISO 16834-A G 89 6 M21 Mn4Ni2CrMo) (Table 3).

Table 3

Chemical composition of UNION X96 wire [13]

C, %	Si, %	Mn, %	Cr, %	Mo, %	Ni, %
0.10	0.81	1.82	0.035	0.61	2.32

Table 4

P3 sample welding parameters

Number of layers	Process	Wire diameter, mm	Amperage, A	Voltage, V	Welding source	Speed, mm/min	Unit energy, kJ/mm
1	135	1.0	102	19.5	DC „+”	240	34

2.2. Methods and scope of the research

Non-destructive tests (NDTs) and destructive tests were performed.

The research included two NDTs:

- Visual tests, according to the EN ISO 17638 standard and the assessment criteria according to EN ISO 5817 norm.
- Magnetic-powder tests, according to the EN ISO 17638 standard and the assessment criteria according to EN ISO 5817 norm.

The destructive tests included:

- Bending with the PN-EN ISO 5173 standard. ZD-40 strength machine was used.
- Microstructure with the Adler reagent; light microscope.
- Hardness tests.

2.3. Results of non-destructive tests

Visual inspections of welds (S1, S2) were done using standard equipment: 3x magnification and a lux-meter (550 Lx). It was observed that the tested welds were made correctly, and the quality was assessed by acceptability limit “B” (PN EN ISO 5817 standards). The magnetic-powder test for samples with a copper backing and without a copper backing (S1 and S2) was run using the wet method (field strength 3.1 kA/m, white light 520 Lx, temperature 21 °C). The results of the NDTs are given in Table 5.

Table 5

Results of the magnetic-powder tests for S1 and S2

Symbol	Detected implications	Test results
S1	Small defects	Negative
S2	No defects	Positive

The results of the magnetic-powder tests of S2 were positive, as no cracks were detected in the HAZ. When welding without a copper washer (S1), small cracks, usually in the HAZ and occasionally in the weld, were observed.

2.4. Results of the strength tests

First, static elongating tests of the specimen without a backing (S1) were performed at ambient temperature on a ZD-100 strength testing machine. Each time, three elongating tests were carried out. The samples were labelled with S1a, S1b and Sc symbols. Test results of tests are shown in Table 6.

It is easy to see that the joint strength is lower (about 750 MPa) than the high strength of the base material (about 1200 MPa). Similarly, three measurements were taken during an elongating test of 1.8 mm-thick S2 samples using copper backing cooling. These samples were labelled S2a, S2b and S2c (Table 7).

Table 6

The results of tensile tests of S1 samples

Value	S1a	S1b	S1c
Fu (MPa)	742	758	749
Fy (MPa)	661	686	682
A ₅ (%)	9.3	9.2	9.2

The data from Table 7 clearly show that the welds were made correctly and that Fy and Fu are at the required high level. For Fy, a minimum of 900 MPa is required according to EN-ISO 15614-1 norm. According to the measurements, Fy was in the range of 801– 823 MPa, while Fu was within the limits of 951– 965 MPa.

The elongation (A₅) in both cases was similar, but a larger value for the S2 samples is noticeable.

Table 7

The results of tensile tests of S2 sheets

Sample	S2a	S2b	S2c
Fu (MPa)	965	954	951
Fy (MPa)	823	809	801
A ₅ (%)	10.5	10.7	10.7

Next, the bending test of S1 and S2 samples (thickness 1.8 mm) was undertaken. The sample had a thickness of a=1.8 mm, a width of b=20 mm, a mandrel of d=14 mm, a spacing of supports of d+3a=31 mm, and a bending angle of 180°. Five bending measurements were taken for each of the tested joints from a root side (S1F and S1R) and from a face side (S2F and S2R samples). The results are summarized in Table 8.

Table 8

Bending results of S1 and S2 samples

Sample	Side of deformation	a × b [mm]	Angle of bending	Observation
S1R	Root	1.8 × 20	180°	Cracks in HAZ
S1F	Face	1.8 × 20	180°	Crack in weld
S2R	Root	1.8 × 20	180°	No cracks
S2F	Face	1.8 × 20	180°	No cracks

Table 8 shows that the bending test of S2 samples was carried out correctly, and the evaluation of the tests was positive without cracks and other discrepancies. In the case of the welding of Docol 1200 M MAG without backings, cracks were observed in both cases (bending from the face and from the side of the root) (Fig. 2a).

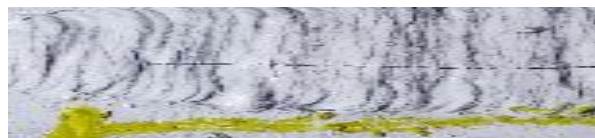


Fig. 2a. Crack in the weld after the bending test; S1

2.5. Metallographic analysis

Metallographic samples were also made, and the structures of 1.8 mm thick joints (S1 and S2) were checked. The structure was different in the two cases. The samples etched in Adler's reagent were observed using the LM (Figs. 3, 4a, and 4b). The structural test results indicate that martensite, bainite and coarse ferrite structure were dominant in the examined joints. This structure can affect the

appearance of cracks in the HAZ. The microstructural results indicate that mainly martensitic and ferritic structures were dominant in the joint. However, the presence of coarse ferrite and bainite is unfavourable in the joint structure with a crack in the HAZ (Fig. 3a). A much more favourable metallographic structure was observed after welding using a copper backing.

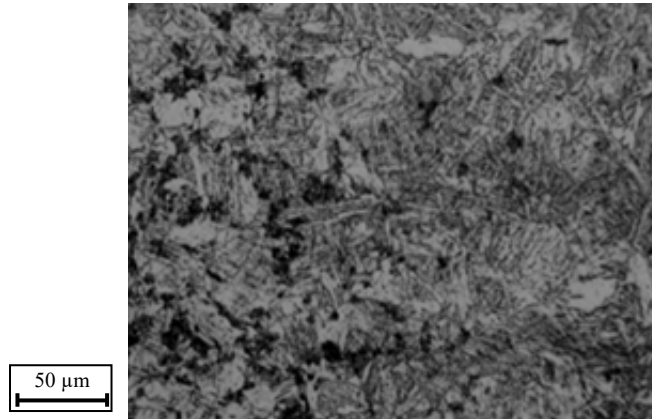


Fig. 3. Microstructure of the weld (S1). Visible: martensite, bainite, coarse ferrite (LM)

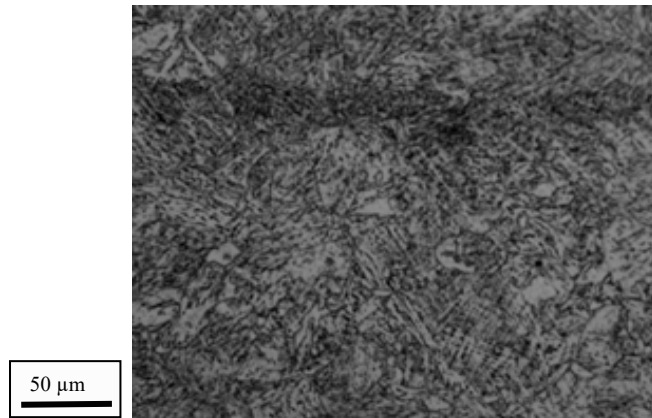


Fig. 4a. Microstructure of the weld (S2). Visible: mainly martensite and rarely fine-grained ferrite (LM)

Additionally, Fig. 4b shows a macrograph of a defect-free joint (S2) with a clearly marked HAZ.



Fig. 4b. Macrograph of the weld (S2) with clearly marked HAZ (in the middle of the photo)

The weld was high quality (i.e. it was free from welding incompatibilities and defects). The structure of tempered martensite was dominant in the HAZ as a result of the effect of heat associated with the laying of successive layers of the weld. Fig. 4c shows the HAZ of partial recrystallization. The joint was made correctly and contained no welding defects or imperfections.

3. NUMERICAL SIMULATIONS

The temperature field was calculated in all parts of the welding process. The phenomenon was modelled as an initial-boundary problem. Due to the nonlinear characteristics of welded materials, the governing differential equation is nonlinear. The boundary conditions were also nonlinear. This problem

was solved by implementing a combination of particular numerical procedures. Numerical simulations were based on the method of fundamental solution [14, 15, 16], supported by Picard iterations and the method of finite differences.

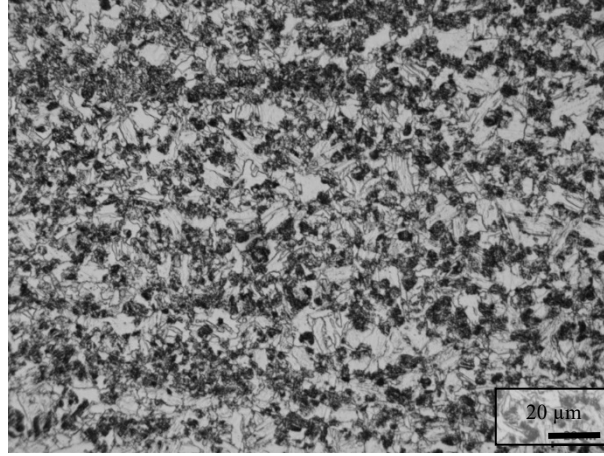


Fig. 4c. HAZ (sample S2)

3.1. Mathematical model

The process of welding yields high temperatures in the welded parts. Therefore, it is necessary to consider the characteristics of materials as functions dependent on temperature. Since the process takes place with very large temperature differences, the relationship between the heat conduction coefficient and temperature is highly nonlinear.

Thermal conductivity [W/(kg K)] is given for used materials as follows:

- the steel plate

$$\tilde{\lambda}_{st}(\tilde{t}) = -3.46498 \cdot 10^{-5} \tilde{t}^2 + 4.862278 \cdot 10^{-2} \tilde{t} + 14.02109 \quad (1)$$

- the weld

$$\tilde{\lambda}_w(\tilde{t}) = -5.189399 \cdot 10^{-5} \tilde{t}^2 + 5.882202 \cdot 10^{-3} \tilde{t} + 20.12045 \quad (2)$$

- the backing (made of copper)

$$\tilde{\lambda}_{co}(\tilde{t}) = 1.014123 \cdot 10^{-6} \tilde{t}^3 - 3.2005579 \cdot 10^{-3} \tilde{t}^2 + 3.37066 \tilde{t} + 873.4965 \quad (3)$$

Specific heat capacity [J/(kg K)]

Since the process takes place with very large temperature differences, the relationship between the specific heat capacity of the plate is calculated as follows:

$$\tilde{c}_{p,st}(\tilde{t}) = 3.003855 \cdot 10^{-9} \tilde{t}^3 - 4.890191 \cdot 10^{-6} \tilde{t}^2 + 2.824982 \cdot 10^{-3} \tilde{t} + 5.527310 \cdot 10^{-2} \quad (4)$$

- the weld

$$\tilde{c}_{p,w}(\tilde{t}) = -3.200329 \cdot 10^{-10} \tilde{t}^3 + 1.040969 \cdot 10^{-6} \tilde{t}^2 - 4.274016 \cdot 10^{-4} \tilde{t} + 0.5083426 \quad (5)$$

- the backing

$$\tilde{c}_{p,co}(\tilde{t}) = -7.322853 \cdot 10^{-8} \tilde{t}^2 + 2.045639 \cdot 10^{-4} \tilde{t} + 0.3555642 \quad (6)$$

Thermal conductivity in general form:

- the steel plate

$$\tilde{\lambda}_{st}(t_{st}) = \tilde{\alpha}_{st} + \tilde{\beta}_{st} t_{st} + \tilde{\gamma}_{st} t_{st}^2 \quad (7)$$

- the weld

$$\tilde{\lambda}_w(t_w) = \tilde{\alpha}_w + \tilde{\beta}_w t_w + \tilde{\gamma}_w t_w^2 \quad (8)$$

- the copper washer

$$\tilde{\lambda}_{co}(t_{co}) = \tilde{\alpha}_{co} + \tilde{\beta}_{co} t_{co} + \tilde{\gamma}_{co} t_{co}^2 + \tilde{\delta}_{co} t_{co}^3 \quad (9)$$

where \tilde{t} is temperature [K].

The mass density of materials is given as follows:

- the steel plate: 7732 [kg/m³]
- the weld: 7844 [kg/m³]
- the washer 8860 [kg/m³]

The nomenclature related to materials zones is indicated in Fig. 5. Due to symmetry, the half of the cross-section perpendicular to the welding line is taken into account.

The governing equations of the transient temperature field are given below:

- the steel plate

$$\tilde{c}_{p,st}(t_{st})\tilde{\rho}_{st}\frac{\partial t_{st}}{\partial t} = \nabla \cdot (\tilde{\lambda}_{st}(t_{st})\nabla t_{st}) \text{ for } (\tilde{x}, \tilde{y}) \in \tilde{\Omega}_{st} \quad (10)$$

- the weld

$$\tilde{c}_{p,w}(t_w)\tilde{\rho}_w\frac{\partial t_w}{\partial t} = \nabla \cdot (\tilde{\lambda}_w(t_w)\nabla t_w) \text{ for } (\tilde{x}, \tilde{y}) \in \tilde{\Omega}_w \quad (11)$$

- the washer

$$\tilde{c}_{p,co}(t_{co})\tilde{\rho}_{co}\frac{\partial t_{co}}{\partial t} = \nabla \cdot (\tilde{\lambda}_{co}(t_{co})\nabla t_{co}) \text{ for } (\tilde{x}, \tilde{y}) \in \tilde{\Omega}_{co} \quad (12)$$

where t_{st} is the temperature in the steel plate [K], t_w is the temperature in the weld [K], t_{co} is the temperature in the washer [K] and t is time.

For this problem, the initial conditions are defined as follows:

- the steel plate

$$t_{st}(\tilde{\mathbf{x}}, t_0) = \tilde{f}_{st}(\tilde{x}, \tilde{y}) \text{ for } (\tilde{x}, \tilde{y}) \in \tilde{\Omega}_{st} \quad (13)$$

- the weld

$$t_w(\tilde{\mathbf{x}}, t_0) = \tilde{f}_w(\tilde{x}, \tilde{y}) \text{ for } (\tilde{x}, \tilde{y}) \in \tilde{\Omega}_w \quad (14)$$

- the washer

$$t_{co}(\tilde{\mathbf{x}}, t_0) = \tilde{f}_{co}(\tilde{x}, \tilde{y}) \text{ for } (\tilde{x}, \tilde{y}) \in \tilde{\Omega}_{co} \quad (15)$$

where $\tilde{\mathbf{x}} = (\tilde{x}, \tilde{y})$. The source function is given for the region of the weld as $\tilde{q}_v(\tilde{\mathbf{x}}, t)$.

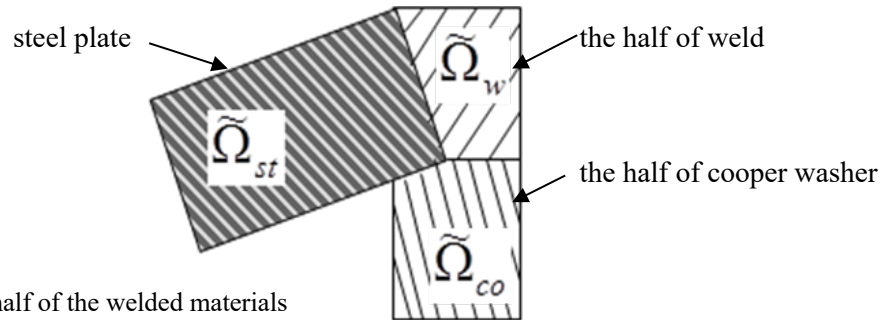


Fig. 5. The geometry of half of the welded materials

Boundary conditions

- the natural convection

$$\frac{\partial t_{st}}{\partial n} = \tilde{\alpha}_{st}(t_{st} - t_{am}) \text{ on } \tilde{\Gamma}_1 \cup \tilde{\Gamma}_4 \quad (16)$$

$$\frac{\partial t_w}{\partial n} = \tilde{\alpha}_w(t_w - t_{am}) \text{ on } \tilde{\Gamma}_8 \quad (17)$$

$$\frac{\partial t_{co}}{\partial n} = \tilde{\alpha}_{co}(t_{co} - t_{am}) \text{ on } \tilde{\Gamma}_9 \cup \tilde{\Gamma}_{10} \quad (18)$$

- the plate temperature

$$t_{st} = t_{plate} \text{ on } \tilde{\Gamma}_5 \quad (19)$$

- the symmetry

$$\frac{\partial t_w}{\partial n} = 0 \text{ on } \tilde{\Gamma}_7 \quad (20)$$

$$\frac{\partial t_{co}}{\partial n} = 0 \text{ on } \tilde{\Gamma}_{11} \quad (21)$$

- the connection between the two regions:

the steel plate and the weld (i.e. on $\tilde{\Gamma}_4$)

$$t_{st} = t_w \quad \tilde{\lambda}_{st}(t_{st}) \frac{\partial t_{st}}{\partial \tilde{n}} = \tilde{\lambda}_w(t_w) \frac{\partial t_w}{\partial \tilde{n}} \quad (22, 23)$$

the steel plate and the washer (i.e. on $\tilde{\Gamma}_3$)

$$t_{st} = t_{co} \quad \tilde{\lambda}_{st}(t_{st}) \frac{\partial t_{st}}{\partial \tilde{n}} = \tilde{\lambda}_{co}(t_{co}) \frac{\partial t_{co}}{\partial \tilde{n}} \quad (24, 25)$$

the weld and the washer (i.e. on $\tilde{\Gamma}_6$)

$$t_w = t_{co} \quad \tilde{\lambda}_w(t_w) \frac{\partial t_w}{\partial \tilde{n}} = \tilde{\lambda}_{co}(t_{co}) \frac{\partial t_{co}}{\partial \tilde{n}} \quad (26, 27)$$

3.2. Numerical procedure and simulation results

The proposed numerical procedure was based on a combination of several numerical methods. Due to the differential with respect to time appearing in Eqs. (10)–(12) The finite difference method is used. The differential with respect to time was approximated by finite differences. Thus, the solution was found in particular time steps. For each time step, the nonlinear boundary value had to be solved. The proposal of this paper is to apply Picard iterations to eliminate nonlinearities in Eqs. (10)–(12) and in the boundary conditions (16–27). In this way, the linear boundary value problems were obtained for each iteration step. Such problems were solved by the method of fundamental solutions supported by the approximation using radial basis functions. This method gives solutions in the form of analytical functions, which are continuous.

The numerical experiment was performed for real data of welded plates. The temperature at the steel plate point $(0.9L, 0.5h)$ is presented in Fig. 6.

In the case without cooling by copper washers, the cooling process took the longest time (more than 12 s). When the copper washer was used, the cooling time was much shorter. For copper plates of double the width equal to $2d$, the time of cooling to 500°C took less than half the cooling time when a copper washer was not applied.

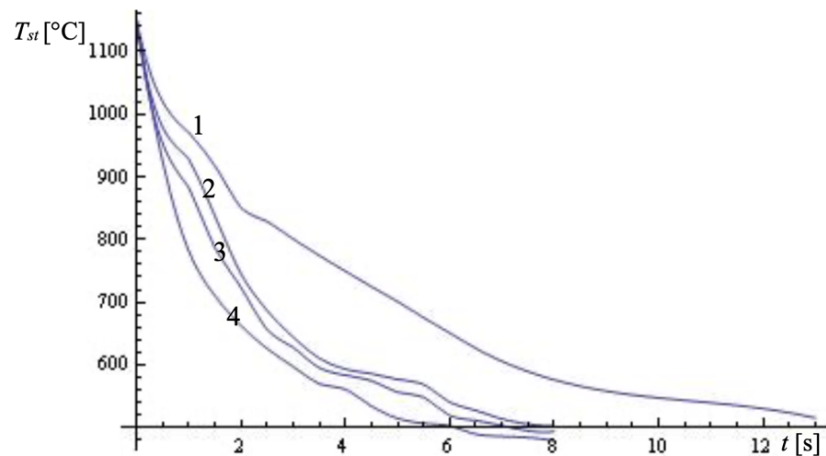


Fig. 6. Temperature at steel plate point (0.9L,0.5h): 1 – without the washer; 2 – with a washer width equal to d ; 3 – with a washer width equal to $1.5d$; 4 – with a washer width equal to $2d$

It is useful to estimate the rate of cooling (RoC), which indicates the most efficient method of cooling after welding. RoC is the fraction of the temperature drop, measured in time intervals. The values of RoC are presented in Table 9.

Table 9

Rate of cooling for welding variants

Welding variant	Rate of cooling [$^{\circ}\text{C}/\text{s}$]	Heat affected zone [%]
1	39.3037	100
2	71.7346	90
3	79.1037	87
4	91.2673	80

In Table 9, the HAZs are estimated as well. The range of HAZs for one variant (without a copper washer) was taken as reference one. The range of HAZs for the most effective cooling case (i.e. that with the highest RoC) was 20% lower than the HAZ for variant 1. This means that the influence of high temperature appearing during welding affected a smaller zone of material in welding variant 4 and that the characteristics of the material were changed in the lower region of the sample. Estimating an HAZ is very important from an engineering point of view. The compatibility of the numerical HAZ range estimation can be seen with in situ surveys. This makes it possible to numerically estimate the behaviour of a welded joint (in this case, welded joints used for the structure of means of transport).

4. CONCLUSIONS

The technique of weight reduction in the automotive industry has attracted special attention for over 20 years [18]. The present article examined the welding of high-strength steels for the structure of means of transport.

AHSS welding is difficult, and the mechanical properties obtained are clearly inferior to those of the base material. In this study, copper backings were used to facilitate the welding process. Their purpose is to form the weld ridge and dissipate heat, leading to a fragmentation of the structure and improved mechanical properties. Computer simulations of the heat flow in the welded joint were performed to provide a more complete understanding of the phenomena occurring in the welded material.

In situ and numerical experiments were performed. The in-situ experiments showed that the welding process introduces changes into the material. The numerical experiment allowed estimates of the geometrical range of the changed material. The HAZ calculations made it possible to identify the geometrical region of the changed material.

The proposed numerical approach is a good tool for predicting welding process parameters (e.g. the width of the cooling plate), which makes it possible to obtain a product with the desired properties. It has been observed that the HAZ in the joint made with a copper backing was narrower than in the case with no backings. For each material and thickness of the welded plate, the proportions of the HAZ were different. However, this issue was not dealt with in this article.

This research solved the material and technological problem of obtaining high-strength welded joints made of Docol 1200 M steel. The obtained solution is important for the structures of means of transport, particularly those subjected to heavy loads.

The solution made it possible to use the material for the construction of mobile platforms and to reduce the weight of the tested means of transport. An example of the use of the developed technology is shown in Fig. 7.

In the future, the authors will work to develop the TTT diagram (also known as time-temperature-transformation) for welding conditions, taking into account various cooling conditions of the joint.



Fig. 7. A mobile platform arm welded using the newly obtained technology

Acknowledgement

The paper corresponds with the COST CA 18223 project and was mainly funded by the Silesian University of Technology (grant number BK-270/RT1/2022) and the Poznan University of Technology (grant number SBAD 0613/SBAD/4710).

References

1. Bleck, W. & Larour, P. & Baeumer, A. High Strain Tensile Testing of Modern Car Body Steels. *Material Forum*. 2005. Vol. 29. P. 21-28.
2. Kowalewski, Z. & Szymczak, T. & Maciejewski, J. Material effects during monotonic-cyclic loading, *Inter. J. Solids Struct.* 2014. Vol. 51. P. 740-753. DOI: <http://dx.doi.org/10.1016/j.ijsolstr.2013.10.040>.
3. Szymczak, T. & Makowska, K. & Kowalewski, Z. Influence of the welding process on the mechanical characteristics and fracture of the S700MC high strength steel under various types of loading. *Materials*. 2020. Vol. 13. No. 5249. P. 1-17. DOI: <https://doi.org/10.3390/ma13225249>.
4. Sanraj Diesel Truck Mounted Mobile Crane, Capacity: 20-25 ton, Platform Height: 80-100 feet. Available at: <https://www.indiamart.com/proddetail/truck-mounted-mobile-crane-21359395330.html>.
5. Barsukov, V. & Tarasiuk, W. & Shapovalov, V. & Krupicz, B. & Barsukov, V.G. Express Evaluation Method of Internal Friction Parameters in Molding Material Briquettes. *Journal of Friction and Wear*. 2017. Vol. 38. No. 1. P. 71-76. DOI: <https://doi.org/10.3103/S1068366617010032>.

- Chatterjee, D. Behind the Development of Advanced High Strength Steel (AHSS) Including Stainless Steel for Automotive and Structural Applications - An Overview. *Materials Science and Metallurgy Engineering*. 2017. Vol. 4. No. 1. P. 1-15. Available at: <http://pubs.sciepub.com/msme/4/1/1/index.html>.
6. Górka, J. & Ozgowicz, A. Robotic welding of high-strength DOCOL 1200M steel with Laser SEAM Stepper system. *Weld. Tech. Rev.* 2017. Vol. 89. No. 10. DOI: <https://doi.org/10.26628/WTR.V89I10.812>.
 7. Hadryś, D. Impact load of welds after micro-jet cooling. *Archives of Metallurgy and Materials*. 2015. Vol. 60. DOI: <https://doi.org/10.1515/amm-2015-0409>.
 8. Górka, J. Assessment of the weldability of T-welded joints in 10 mm Thick TMCP steel using laser beam. *Materials*. 2018. Vol. 11. No. 7. P. 1192-1202. DOI: <https://doi.org/10.3390/ma11071192>.
 9. Darabi, J. & Ekula, K. Development of a chip-integrated micro cooling device. *Microelectronics Journal*. 2003. Vol. 34. No. 11. P. 1067-1074. DOI: <https://doi.org/10.1016/j.mejo.2003.09.010>.
 10. Muszynski, T. & Mikielewicz, D. Structural optimization of microjet array cooling system. *Applied Thermal Engineering*. 2017. Vol. 123. P. 103-110. DOI: <https://doi.org/10.1016/j.applthermaleng.2017.05.082>.
 11. Celin, R. & Burja, J. Effect of cooling rates on the weld heat affected zone coarse grain microstructure. *Metallurgical and Materials Engineering*. 2018. Vol. 24. No. 1. P. 37-44. DOI: <https://doi.org/10.30544/342>.
 12. Tarasiuk, W. & Szymczak, T. & Borawski, A. Investigation of surface after erosion using optical profilometry technique, *Metrology and Measurement Systems*. 2020. Vol. 27. No. 2. P. 265-273. DOI: <https://doi.org/10.24425/mms.2020.132773>.
 13. Hashimoto, F. & Lahoti, G.D. Optimization of Set-up Conditions for Stability of The Centerless Grinding Process. *CIRP Annals - Manufacturing Technology*. 2004. Vol. 53. No. 1. P. 271-274. DOI: [https://doi.org/10.1016/S0007-8506\(07\)60696-9](https://doi.org/10.1016/S0007-8506(07)60696-9).
 14. Bradley, J.R. & Aaronson, H.I. Growth kinetics of grain boundary ferrite allotriomorphs in Fe-C-X alloys. *Metallurgical Transactions A*. 1981. Vol. 12. P. 1729-1741.
 15. Jurek, A. *Increasing the operating range of the mobile platform for motor vehicles while maintaining the curb weight*. PhD theses. 2022. Silesian University of Technology [In Polish: *Zwiększenie zasięgu operacyjnego podestu ruchomego pojazdów samochodowych przy zachowaniu masy własnej pojazdu*].
 16. Demeri, M.Y. *Advanced High-Strength Steels. Science, Technology, and Applications*. ASM Technical Books. OH: ASM International. 2013. DOI: <https://doi.org/10.31399/asm.tb.ahsssta.9781627082792>.
 17. Earmi, M. & Anok, M. & Roosimolder, L. Weith reduction of support structures. In: *DS 49: Proceedings of Nord-Design 2004 Conference*. Tampere, Finland, 2004. P 309-324.

Received 16.12.2020; accepted in revised form 26.08.2022